scientific reports

Check for updates

OPEN

Circulating tumor cell–derived lines exhibit an amoeboid mode of migration

Guillaume Belthier[1,17], Veronika te Boekhorst[2,3,17], Zeinab Homayed[1], Jihane Vitre Boubaker[1], Fanny Grillet[1], Marie Alexandra Albaret[4,5,6], Momeneh Foroutan[7,8], Geneviève De Sousa[4,5,6], Lucile Canterel-Thouennon[9], Jean-François Bourgaux[10], Michel Prudhomme[11], Emmanuelle Samalin[1,12], Thibault Mazard[12], Gérard Lossaint[12], Lakhdar Khellaf[13,14,15], Frédéric Hollande[7,8], Hichem C. Mertani[4,5,6,7], Peter Friedl[2,3,16,17] & Julie Pannequin[1,17]✉

Epithelial-to-mesenchymal transition (EMT) has been described as a critical step in the metastatic process. Recent studies have detected circulating tumor cells (CTCs) in hybrid EMT-states in the blood of cancer patients, however fully epithelial CTC states were also detected, challenging the EMT dogma. Besides invasion through EMT, the amoeboid migration mode has been proposed as an alternative migration mechanism for CTCs, but functional evidence is lacking. In this study, we aimed to investigate the migration mode retained in established CTC lines using in vitro and in vivo assays as well as patient samples. We found that established CTCs are strictly epithelial and yet develop blebbing-amoeboid movement in 3D environments, including individual as well as amoeboid-collective migration modes. Thus, clinically isolated CTCs from epithelial cancer patients retain a range of invasion strategies during metastasis, including amoeboid dissemination.

Keywords Circulating tumor cells, Amoeboid migration, Colorectal cancer, Metastasis, Mouse models, Human sections

The vast majority of cancer related deaths result from distant organ metastasis[1]. Colorectal cancer (CRC) is one of the most frequent cancers with almost 2 million new CRC cases diagnosed and approximately 1 million caused deaths in 2020 worldwide[2]. The overall 5-year survival stands at 65%. However, for patients with localized stage colorectal cancer, it reaches 91%, dropping sharply to 14% when the tumor has metastasized[3]. Deciphering mechanisms involved in the metastatic process has become urgently needed to propose alternative therapeutic strategies. One of the least understood stages of the metastatic process is the transition from the primary site to organ colonization, mediated by circulation of tumor cells within the bloodstream which may retain or not features acquired in the primary tumor microenvironment. Circulating tumor cell (CTC) counting has been proposed as a promising biomarker in many cancers including CRC[4], with EpCAM positive cell enumeration as an FDA-approved prognostic marker (CellSearch®, Veridex). However, CTC phenotypic characterization has

[1]Institut de Génomique Fonctionnelle, Univ. Montpellier, CNRS, INSERM, Montpellier, France. [2]David H. Koch Center for Applied Research of Genitourinary Cancers, The University of Texas MD Anderson Cancer Center, Houston, TX, USA. [3]Department of Cell Biology, Radboud University Medical Centre, 6525 GA Nijmegen, the Netherlands. [4]Inserm U1052, UMR5286 Centre de Recherche en Cancérologie de Lyon, CNRS, 69000 Lyon, France. [5]Centre Léon Bérard, 69008 Lyon, France. [6]Université de Lyon 1, 69000 Lyon, France. [7]Plasticity, Heterogeneity and Tumour Microenvironment, International Research Laboratory – PHANTOM - CNRS and The University of Melbourne, Department of Clinical Pathology, Victorian Comprehensive Cancer Centre, The University of Melbourne, Melbourne, VIC 3010, Australia. [8]Collaborative Centre for Genomic Cancer Medicine, Victorian Comprehensive Cancer Centre, Melbourne, VIC, Australia. [9]Plateforme MPCC—SIRIC Montpellier Cancer, IRCM, Montpellier, France. [10]Service d'Hépato-Gastroentérologie, CHU Carémeau, Nîmes, France. [11]Service de Chirurgie Digestive, CHU Carémeau, Nîmes, France. [12]Medical Oncology Department, Institut du Cancer de Montpellier (ICM), University Montpellier, 34298 Montpellier, France. [13]Institut Régional du Cancer de Montpellier (ICM)-Val d'Aurelle, Montpellier, France. [14]Tumor Microenvironment and Resistance to Treatment Lab, INSERM U1194, Montpellier, France. [15]Université de Montpellier, Montpellier, France. [16]Cancer Genomics Center, 3584 CG Utrecht, the Netherlands. [17]Guillaume Belthier, Veronika te Boekhorst, Peter Friedl and Julie Pannequin equally contributed to this work. ✉email: julie.pannequin@igf.cnrs.fr

been initiated with the ability to amplify these cells in culture[5,6]. In this context, we have been the first to amplify several CTC lines from the blood of patients with metastatic colorectal cancer[7].

Epithelial to mesenchymal transition (EMT) as a mandatory step in the metastatic process is still controversial[8,9]. In fact, epithelial, mesenchymal and hybrid phenotypes have been detected in CTCs isolated from patients with different tumor types[10,11]. Mesenchymal single cells use integrins and metalloprotease-dependent degradation of the extracellular matrix (ECM) to invade the surrounding stroma and get access to vessels for dissemination[12]. Distinct from cells with the mesenchymal phenotype, amoeboid migration, also used by immune cells, is another type of tumor cell migration[13]. It relies on changes in cell shape and changes in actin architecture to squeeze between the ECM but does not depend on integrins and proteolytic degradation of ECM[14]. Concomitantly with the downregulation of metalloprotease (MMPs) and integrin expression, upregulation of the Rho/ROCK signaling pathway leads to mesenchymal-amoeboid transition (MAT)[15–19]. However, epithelial cancer cells are not required to undergo EMT to acquire an amoeboid migration, they can also undergo epithelial-ameboid transition (EAT)[20].

Using different CTC lines previously established from metastatic colorectal cancer patients[7], we questioned their mode of migration. As a dominant shared characteristic, CRC-CTCs maintained a strong epithelial phenotype. Many studies have speculated that CTC could use an amoeboid mode of migration[21,22], but because of the lack of relevant models no phenotypical proof has been described. Using standard CRC cell lines, primary samples, and CTC lines established in our laboratory, our colleagues were the first to show that cancer cells can migrate collectively in an amoeboid-like manner.[23]. In the present work, we exploit the unique model of CTC lines to further test whether cell individualization depends on amoeboid or rather EMT-related strategies. Using in vitro *and* in vivo models as well as ex vivo patient tumor samples, we show that CTCs employ both individual and collective amoeboid modes of migration, similar to macrophages or other immune populations, supporting a concept of diversity of cancer invasion strategies.

Results

CTCs display a phenotypic plastic signature and express epithelial markers

To understand which migration mode is used by CTCs, we interrogate the transcriptomes of the CTCs derived from patients 44 (CTC44) and 45 (CTC45) and compare it to the cell line established from the primary tumor of patient 44 (CPP44)[7] (Table1). The 3 cell lines were scored against Epithelial, Mesenchymal, TGFb-induced EMT and Mesenchymal Amoeboid Transition (MAT) signatures using sIngscore[24–27] (Fig. 1A). Results highlighted first the contrast between the high Epithelial feature of CTCs and the strong mesenchymal/EMT characteristics of matching primary tumor cells established from patient 44. The second interesting observation made by comparing the expression profile of the 3 cell lines for the MAT features is that CTCs may have acquired an amoeboid program instead of retaining the mesenchymal program to migrate and circulate.

To go deeper in the phenotypic characterization of the patient derived CTCs, we compared the expression of epithelial and mesenchymal markers at the mRNA and protein level in two circulating tumor cell lines (CTC44 and CTC45) with a primary tumor cell line (CPP44) and a liver metastasis tumor cell line (CPP45). CTC45 and CPP45 have been established from the same patient but the first line is from the blood and the second is from a liver metastasis (Table1). Fig. 1B shows that CTC lines express high levels of the epithelial marker E-cadherin mRNA but not the mesenchymal markers, Vimentin and Zeb-1. Conversely, cell lines from primary tumor and liver metastasis (CPP44 and CPP45) exhibit higher mRNA expression level for the mesenchymal genes, especially in the case of CPP45. In particular, CPP45 has a higher Vimentin expression suggesting to be further committed in the EMT process compared to CPP44. At the protein level, Fig. 1C confirms the epithelial phenotype of the 2 CTC lines and the mesenchymal phenotypes of the corresponding CPP lines. We previously characterized the strong metastatic initiating potential of CTC44 and CTC45 [7] but the total absence of mesenchymal phenotype in both lines was unexpected according to the metastatic cascade. Taken together, these results suggest an epithelial migration independent of mesenchymal trait but probably by using an amoeboid migration mode. To validate this Epithelial-amoeboid phenotype, we stained both CTC lines and the corresponding CPP lines with the epithelial marker EpCAM and the phosphorylated form of myosin light chain 2 (pMLC2), specific for amoeboid phenotype[28]. The phosphorylation and membrane localization of MLC2 is visible only for the 2 CTC lines and not for the corresponding CPP lines (Fig. 1D). Altogether these results suggest that CTCs derived from patient blood samples have a strong epithelial phenotype.

CTC harbor functional amoeboid features

We then further characterized whether the molecular program translates to functional amoeboid migration using in vitro assays and incorporating a recently established CTC line (here called CTC31)[29] alongside the previously published CTC lines[7]. Of note, we confirmed that the line CTC31 is strongly expressing the epithelial marker EpCAM (Figure S1A). CTC lines were embedded as single cells within a 3D collagen matrix. Remarkably,

Patient #	Origin of the established line			Protocol code
	Primary CRC	Blood	CRC liver metastasis	
31	-	CTC31	-	2016-A00080-51
44	CPP44	CTC44	-	#NCT01577511
45	-	CTC45	CPP45	#NCT01577511

Table 1. Origin of the established cell lines.

these CTCs exhibited a rapid proliferation (average increased volume by 6.9 in 5 days for CTC31 and by 8.9 and 10.5 in 4 days for CTC44 and CTC45 respectively), characterized by the formation of distinct clusters (Figure S1B, C). Despite the scarcity of moving cells and their low speed of migration, we were able to observe single cells (Fig. 2A, B) adopting a blebbing movement toward the collagen (Video 1) with a median migration speed between 0.032 and 0.057 µm/min (Fig. 2C). During migration, the aspect ratio of individually moving CTCs consistently retained a roundish shape and showed blebbing protrusions toward direction of migration (Fig. 2B-E & Figure S1C, D). When grown as small cluster, CTC clusters moved (Fig. 2F & Video 2) at low speed below 0.1 µm/min (Fig. 2G). This speed range matches with collective migration speeds reported in vivo[30] or in vitro[31]. Importantly, migration speed, measured in PEG-coated microchannels by Pages et al., indicates a similar speed between the CTC lines and other epithelial CRC lines (excepted to HT29 which are migrating faster)[23], and the average speed is comparable to our measure in collagen drops. Similarly clustered moving CTCs adopt a roundish shape (Fig. 2H and I). Specific expression of pMLC2 at the membrane (Fig. 1D), cell blebbing and round shape during migration supported our hypothesis based on the CTC RNA signature (Fig. 1A). To functionally test the amoeboid migration, we performed migration assays by impedancemetry on the 3 CTCs lines, as well as on a mesenchymal non-amoeboid cancer cell line (MDA-MB-231-negative control) and an amoeboid T-cell line (Jurkat-positive control)[32]. Migration ability for each cell line was tested in the presence or absence of Y27632, a well-known ROCK inhibitor impacting amoeboid migration[15]. Fig. 2J shows that after 22 h, Y27632 markedly inhibits the migration of CTC45, to an extent comparable to that observed in Jurkat cells. Similarly, migration of CTC44 and CTC31 is affected by ROCK inhibition. Inversely, Y27632 did not impair the mesenchymal MDA-MD-231 cell migration (Fig. 2J). Taken together, after exposure to 3D matrix environments, CTCs retain an amoeboid migration mode.

Amoeboid phenotypes retained in xenograft model tumors

To determine whether the bleb-based migration observed in vitro is recapitulated in a complex tissue environment, we employed in vivo xenograft models. First, CTC lines were subcutaneously xenografted in the flank of immunodeficient mice. Tumor sections were then stained with CK20 antibody to specifically track CTCs with an intestinal marker. Analysis of staining reported that single cells and small multi-cell clusters ("nests") were detached from the tumor bulk and invading the surrounding stroma (Fig. 3A & Figure S2A). Moreover, detached single cells exhibited a round shape compared to neighboring mouse fibroblasts (Fig. 3B). To confirm these observations in an orthotopic model representing the tissue of origin and cell fate, we injected CTC lines into the caecum of immunodeficient mice. This model recapitulates human pathology steps, including primary tumor formation followed by systemic dissemination and the development of lymph nodes, liver and lung metastasis. To distinguish the primary tumor and surrounding single or clustered cells invading the mouse intestine, CK20 and the specific human mitochondrial protein (P-Mito) were detected by immunohistochemistry. CK20 is a specific cytokeratin for intestinal cells and P-Mito cannot be detected in mouse cells, both highlighting only the CTCs injected since they are human cells from a colorectal tumor. Moreover, a cancer cell losing the expression of CK20 can be still detected with the P-Mito antibody. These stainings enabled us to observe invasive ce lls in lymph nodes as well as liver and lung metastasis with the same pattern as the primary tumor: a tumor bulk and single or clustered cells invading the surrounding stroma (Fig. 3C & Figure S2B). In both primary and distant sites, compared to mouse fibroblasts from the caecum, CTCs kept a round shape throughout the dissemination process (Fig. 3D). Of note, immuno-fluorescent staining for E-cadherin and Ki67 on the caecum injected with CTCs showed that the tumor bulk as well as disseminated cluster of cancer cells are epithelial and highly proliferative (Figure S2C) consistent to the phenotypes observed in vitro (Fig. 1B, C and Fig. 2C, G). Thus, CK20 and E-cadherin expression maintenance combined with the round shape of the single and clustered cells across organ types indicates that the amoeboid traits of the CTC lines are an intrinsic phenotype rather than imposed by the tumor stroma.

Amoeboid phenotypes in patient tumor samples

To finally validate the CTC amoeboid trait, we went back to the origin of the CTC lines, i.e., the patient donors. Considering that cell lines established either from the primary tumor of patient 44 or from the liver metastasis of patient 45 display a mesenchymal phenotype, it is reasonable to assume that both the primary tumors and metastases contained a tumor cell population also able to undergoing EMT and/or MET. However, the establishment of epithelial CTC lines intrinsically displaying an amoeboid phenotype from the blood of these patients also may indicate that a subset of cells underwent EAT. In sections of tumor and metastasis surgical excisions, we performed a CK20 staining and detected single and clustered cells surrounding stroma of both primary tumors and metastasis (Fig. 4A). Importantly, these cells exhibited a round shape compared to colon fibroblasts (Fig. 4B), as observed in in vitro and in vivo models indicating intrinsic amoeboid traits. Taken together, these observations made on patient samples confirmed that colorectal primary tumors contain epithelial cells that use amoeboid migration to reach the blood vasculature and some of these CTC ultimately succeed to form liver metastasis in which amoeboid migration also occurs.

Discussion

Cell invasion and migration towards and from blood vessels are key steps during the metastatic cascade. To further functionally characterize colorectal circulating tumor cells (CTCs), which are the culprit of metastasis development, this study used complementary and relevant in vitro approaches along with in vivo and ex vivo models. Based on three established CTC lines from the blood of CRC patients (Table1), their initial characterization indicated that they display metastatic cancer stem cell (CSC) features while maintaining epithelial intestinal protein expression[7,29]. However, the literature mainly associates the gain of CSC and migration phenotype to cancer cells undergoing epithelial to mesenchymal transition (EMT)[33,34].

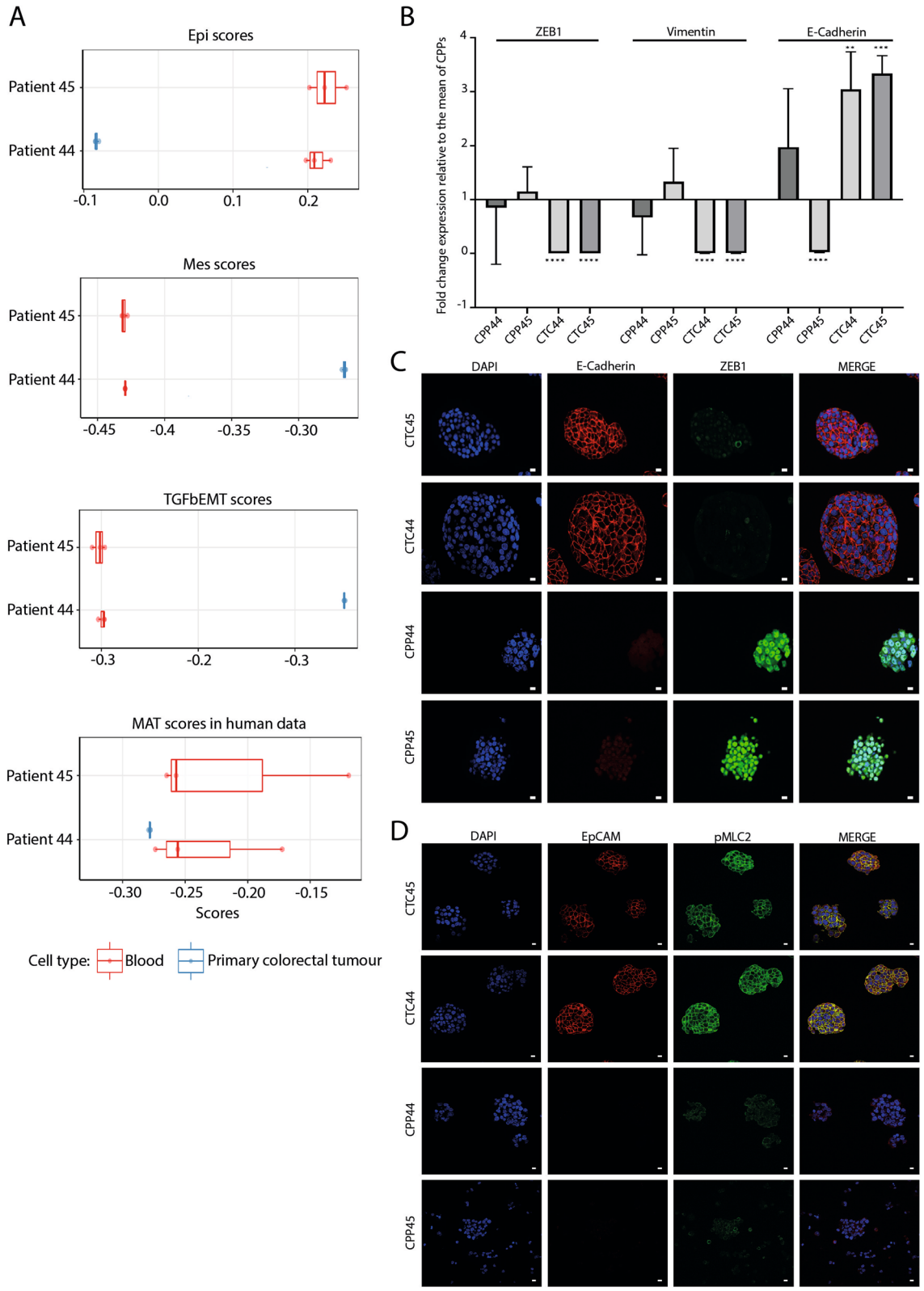

It is well established that within primary tumors, only a small fraction of cells undergoes EMT, and this process is highly dependent on specific microenvironmental cues. Our findings are consistent with this concept and suggest that circulating tumor cells represent a selected subpopulation that does not rely on a full EMT program to achieve migratory competence. Instead, the CTCs analyzed in this study retain amoeboid traits, characterized by rounded morphology, supporting the notion that tumor cell dissemination can occur through alternative modes of motility, highlighting the plasticity of migratory strategies employed by rare tumor cell subsets rather than a uniform transition across the primary tumor mass. Here, both at the gene expression and protein levels, our results not only confirmed the presence of epithelial features as previously described, but

◀**Fig. 1**. CTC lines do not exhibit a mesenchymal but an epithelio-amoeboid phenotype. (**A**) Boxplots representing the singscore value for CTCs (red) from patient 44 and 45 and a tumor cell line from primary tumor of patient 44 (CRC, blue) against epithelial, Mesenchymal, TGFβ EMT and MAT signatures, represented as median score, 25–75 percentile and 1.5X interquartile ranges. (**B**) Fold change expression of mRNAs encoding proteins known as mesenchymal markers (Zeb1 and Vimentin) or an epithelial marker (E-cadherin) relative to the mean of combined CPP44 and CPP45 cell lines. mRNA expression in each cell line was normalized to GAPDH. Results are expressed as mean + -SD, n = 3, student t-test. (**C**) Immunofluorescent staining of representative tumor spheres derived from single-cell (scale bar 10 µm). Names of stained epithelial (E-Cadherin), mesenchymal (ZEB1) markers are specified above each column for the corresponding color. (**D**) Immunofluorescent staining of representative tumor spheres derived from single-cell (scale bar 10 µm). Names of stained epithelial (EpCAM) and amoeboid (pMLC2) markers are specified above each column for the corresponding color.

also clearly indicated the absence of a mesenchymal signature. Of note, another mode of migration initially described for amoebas and then for immune cells, was also described as an alternative migration mode for cancer cells[13,20,31,35,36]. Depending on the context, cancer cells use different types of migration: mesenchymal or amoeboid migration. Moreover, cancer cells can migrate collectively with tip leader cells partially mesenchymal and pulling a queue of epithelial cells or can migrate solitary with either a mesenchymal migration or an amoeboid migration[18,19,36]. For the latest one, existing literature suggests that cancer cells initially undergo EMT process, followed by another potential step termed mesenchymal to amoeboid transition (MAT). This second transition is promoted once cancer cells have to move toward a very confined space or when the environment is not in favor of ECM rearrangement and focal adhesion or upon hypoxic conditions[31,36]. Therefore, EMT was thought to increase the dissemination while MAT increases cell motility under specific confinement contexts like intravasation and extravasation[37]. To elucidate this discrepancy between the literature and the stable CSC-epithelial phenotype of our CTC lines and the requirement to be able to migrate before and after circulation, we compare the gene profile of two CTC lines with one of the corresponding lines established from the primary tumor. Interrogating different gene profiles (as Epi and MAT score) and the membrane localization of pMLC2, we get a first indication of an epithelial-amoeboid phenotype through an epithelial to amoeboid transition (EAT) regardless of mesenchymal features.

In vitro, experiments confirmed the CTC's ability to maintain a round shape and exhibit blebs, allowing them to migrate as single or clustered epithelial cells. Although the measure of the migration speed were not in the same experimental conditions between us and Pages et al., our 3 CTC lines compared to the commercial CRC line HT29[23], are around half slower. However, the migration speed of CTC44 and CTC45 measure by Pages et al. is in the same range than in our experimental condition, confirming the relative slow migration speed of CTCs compare to HT29 but not to other epithelial colorectal cell lines. The high proliferation rate of these CTC lines observed in the orthotopic xenograft model as well as in vitro might be an explanation for their relatively slow migration speed in vitro. Additionally, by targeting the amoeboid migration via the ROCK inhibitor Y27632, CTC31 and CTC44 lines experienced an important reduction of their migratory ability and a drastically loss of migratory ability in the case of CTC45 line. Some of these aspects were confirmed in vivo with different xenograft models. Finally, in patient tissue sections from primary tumor and liver metastasis excisions, we also observed a similar pattern, suggesting a direct EAT for single and cluster cells.

However, unlike in vitro findings, our in vivo observations do not exclude the possibility that column-like structures are masked by tissue sectioning. To conclusively demonstrate the detachment of cancer cells from the tumor bulk through amoeboid-like migration, future studies will require tissue-clearing approaches applied to a broad range of mouse and human tumor samples.

Taking all together, our results highlight a single and collective amoeboid migration acquired before circulation and stably maintained by these cells on top of the stable CSC-epithelial phenotype[7]. Previous studies had linked stem-cell properties or gain of stem-cell properties with amoeboid migrations[38–40]. However, these studies were done with non-epithelial tumor cells, meaning that they undergo in MAT. Additionally, the vast majority of studies describing amoeboid migration on epithelial cancer cells indicate a mandatory EMT initiation[31,36,41–43]. Few works showed a direct EAT[44,45] and it has been described as a response pattern to hypoxic stress in 3D culture[31,36] which induces a memory effect and strongly enhances the metastatic competence[36]. Importantly, all of the works referring to EAT where done only in vitro and without any indication of a stemness phenotype.

To date, only Graziani and colleagues have linked in vitro, gain of stem cell potential with amoeboid features not only on a mesenchymal cancer cell line but also on an epithelial cancer cell line[42]. Interestingly, these two aspects were stable on both cell types and caused by the expression of the oncogene RASSF1C. In line with their results, our present work is the first to show a stable CSC-epithelial phenotype with an amoeboid mode of migration on human ex vivo samples and on human colorectal CTC lines. Additionally, our results indicate that these traits acquired in the primary tumor and are maintained even after distant colonization affecting both single and clustered colon cancer cells. The stability of colorectal CTC lines migration and CSC-epithelial phenotype over many passages in vitro as well as after xenograft transplantation could be caused by the shared mutation *BRAF* V600E[7,29] inducing a similar effect on the Rho/ROCK/MLC2 pathway as RASSF1C does. This hypothesis is also supported by the absence of *BRAF* V600E mutation in both CPP44 and CPP45 mesenchymal cell lines. Targeting this pathway with the ROCK inhibitor Y27632 combined with a BRAF inhibitor could impair the dissemination of a subpopulation with a very high metastatic initiation potential.

Finally, it has been recently described with microchannel chambers that amoeboid migration is compatible with collective migration[23]. We confirmed it with embedded CTCs in collagen, but we also show it for the

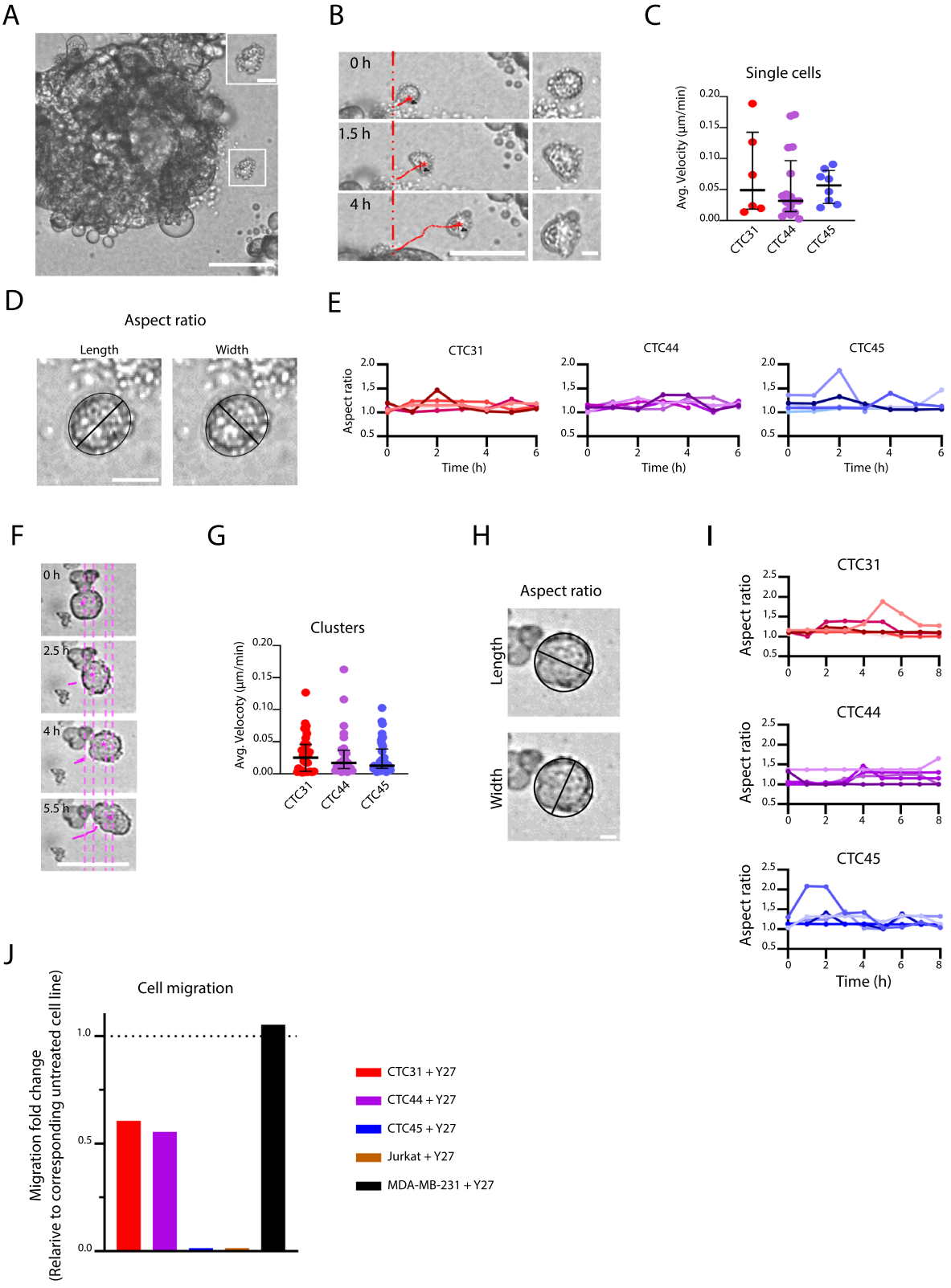

first time from different xenograft mouse models. Confirmation of the potential connection between epithelial-CSC phenotype and amoeboid migration on established CTC lines from other cancers will be the first step in paving the way to pharmaceutical inhibitors blocking the migration of these circulating culprits with a very high potential of metastasis initiation without impacting immune cells.

Methods

Cell line and culture

CTCs and CPPs have been established and cultured as previously reported[7,29].

◀**Fig. 2**. CTC lines use an amoeboid migration mode in vitro. (**A**) Representative bright field micrograph overview of a large CTC31 cluster growing for 3 days in 1.6 mg bovine collagen with a round-blebbing single cell. Scale bar, 50 µm and inset 10 µm. (**B**) Migration path and morphology of a single CTC31 cell detached from a cluster and migrating in 1.6 mg bovine collagen. Vertical dotted red line represents the origin after detachment from the spheroid; red line, path of migration. Scale bar, 50 µm and inset 10 µm. (**C**) Migration velocities single CTCs after 3–4 days (CTC31) or 3–7 days (CTC44 and CTC45) in collagen culture (1.6 mg bovine collagen), obtained by tracking of the centroid over 4 h time period (red line). Data represent the average velocity (excl. non-moving moments) of single cells; horizontal lines, and medians with interquartile range. CTC31, 6 cells; CTC44, 17 cells; CTC45, 8 cells from two independent experiments. (**D**) Representative single CTC aspect ratio (length divided by width, top panel) measured by the elliptical tool in Fiji as an indicator for roundness (Scale bar, 10 µm). (**E**) Aspect ratio over time of single detached CTCs migrating in collagen culture. One line represents one cell followed over 4–6 h. 5 cells for each CTC line. (**F**) Representative bright field micrographs of a CTC31 cluster at 48 h migrating in 1.6 mg bovine collagen monitored for 20 h by timelapse microscopy. Scale bar, 100 µm. (**G**) Migration velocities of CTC clusters after 48 h (CTC31) and 72 h (CTC44 and CTC45) in collagen culture (1.6 mg bovine collagen). Data show the average migration velocities (excl. non-moving moments) of single clusters; horizontal lines, and medians with interquartile range. CTC31, 35 clusters; CTC44, 21 clusters; CTC45, 26 clusters from 2–3 independent experiments. (**H**) Aspect ratio measured with the elliptical tool using Fiji indicating roundness (Scale bar, 10 µm) and (**I**) Aspect ratio over time of spheres migrating in collagen culture (1.6 mg bovine collagen). One line represents one cluster followed over 8 h. 5 clusters for each CTC line. (**J**) Representative real-time analysis using the X-CELLigence system. Fold change of Cell Index upon Rho-ROCK (Y27) inhibitor relative to the corresponding cell line without inhibitor after 24 h of impedance recording. Jurkat and MDA-MB-231 cell lines are used as internal positive and negative controls respectively.

MDA-MB-231 and Jurkat cell lines were purchased from ATCC (HTB-26 ™ and TIB-152 respectively). Briefly, cells are seeded as single cells in suspension resuspended in M12 medium (1 mL/well) in ultra-low attachment 24-well plates (Corning). M12 medium contains advanced DMEM-F12 (Gibco), 2 mmol/L of L-glutamine, 100 Unit/mL of penicillin and streptomycin, N2 supplement (Gibco), 20 ng/mL of epidermal growth factor (R&D) and 10 ng/mL of fibroblast growth factor-basic (R&D). All cell lines were cultured at 37^0 C and 5% CO_2.

qPCR

Total RNA was extracted using the RNeasy mini kit (Qiagen) with DNAse-I treatment. The first strand cDNA was synthesized using Superscript II (Invitrogen) according to the manufacturer's protocol. Each cDNA sample was amplified in triplicates using SYBR Green (Roche) on the LC480 real-time PCR system for gene expression measurement. GAPDH was used as an endogenous control to normalize all the samples. The fold changes in genes expression were calculated with the 2-ΔΔCt method. Primer sequences: GAPDH: Forward: GGTGGTCT CCTCTGACTTCAACA Reverse: GTTGCTGTAGCCAAATTCGTTGT; Vimentin: Forward: TGGCCGACGC CATCAACACC Reverse: CACCTCGACGCGGGCTTTGT; ZEB1: TGCACTGAGTGTGGAAAAGC Reverse: TGGTGATGCTGAAAGAGACG; Ecadherin: Forward: CGAGAGCTACACGTTCACGG Reverse: GGGTGTC GAGGGAAAAATAGG.

Immunofluorescence

FFPE-embedded sample slides were initially dewaxed by heating at 56 °C and then immersed in serial xylene and graded ethanol baths.

For immunofluorescence, antigen retrieval was conducted by boiling slides in citrate buffer (PH 6) for 20 min, followed by blocking non-specific binding sites for 1 h in Phosphate Buffered Saline (PBS) with 10% Donkey serum and 0.5% Triton X-100. Primary antibodies: anti-zeb1 (Bio Techne NBP1-88,845 ; 1/200), anti- Ecadherin (BD Biosciences 610,181 ; 1/200), anti-Ki67 (Abcam ab16667 ; 1/500), anti- EpCAM (proteintech 21,050–1-AP; 1/500), anti- pMLC2(S19) (Cell signaling 1/200) were diluted in blocking buffer and incubated overnight at 4 °C. Fluorescent secondary antibodies (donkey IgG anti-rabbit AF488, donkey IgG anti-mouse AF568, donkey IgG anti-rabbit AF674 and donkey IgG anti-mouse AF488 from Jackson ImmunoResearch) were applied after washing, followed by DAPI staining for nuclei and mounting with fluoromount G. Imaging was performed using an epifluorescent microscope (Zeiss AxioImager Z1 apotome).

Amoeboid signature analysis

The feature count format of the RNA-seq data [BioProject: PRJNA384289][7] was processed using the edgeR package[46] to perform gene filtration, TMM normalization and logRPKM calculation. We then used the singscore package[27] to score patient 44 and patient 45 using their logRPKM values against several signatures, including Epithelial and Mesenchymal signatures[24], TGFb-induced EMT signature[25], and Mesenchymal Amoeboid Transition (MAT) signature[26].

We used ggplot2 package to visualize sample scores as boxplots, where the middle line shows median scores, the two hinges represent 25%- and 75%-tile of the scores, and the two whiskers represent the min score within 1.5 times the interquartile (IQR) range under 25%-tile and the max score within 1.5 times the IQR range over 75%-tile of scores.

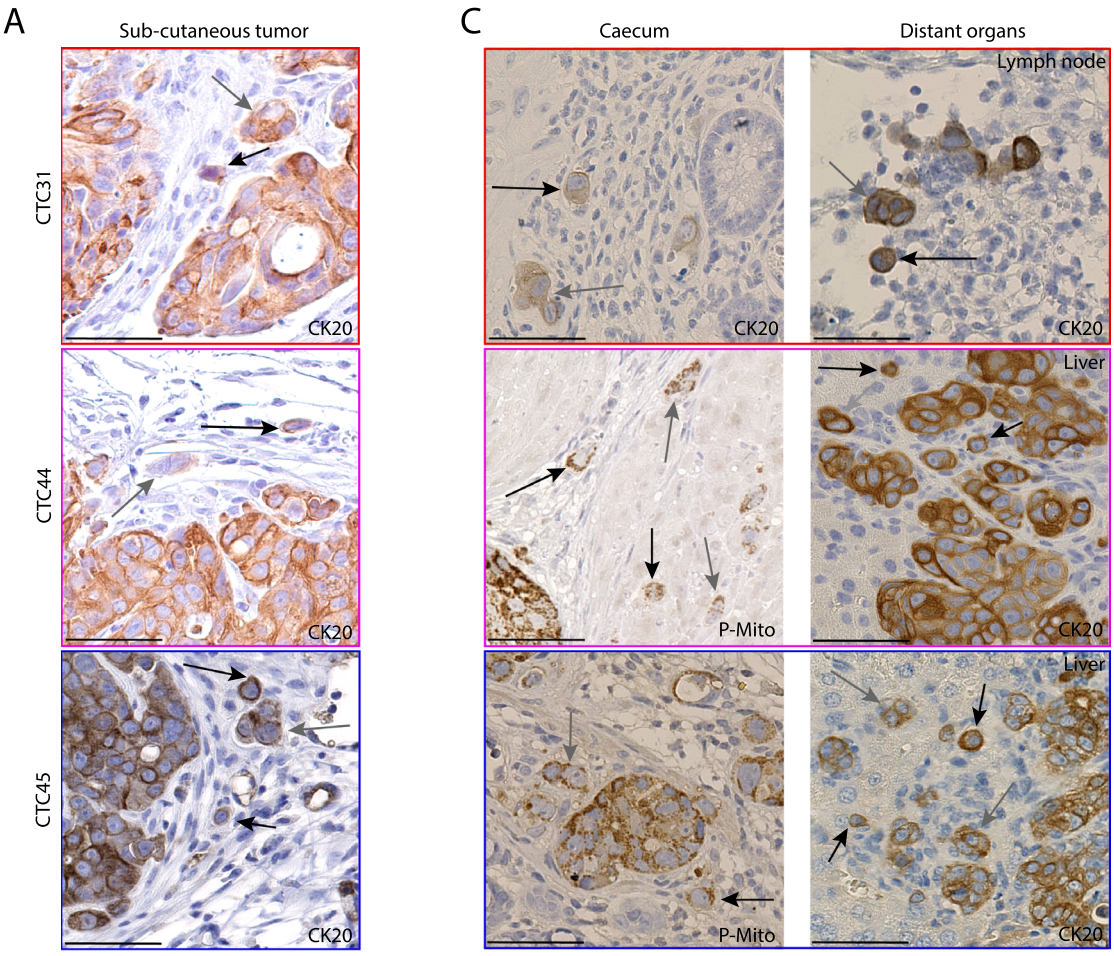

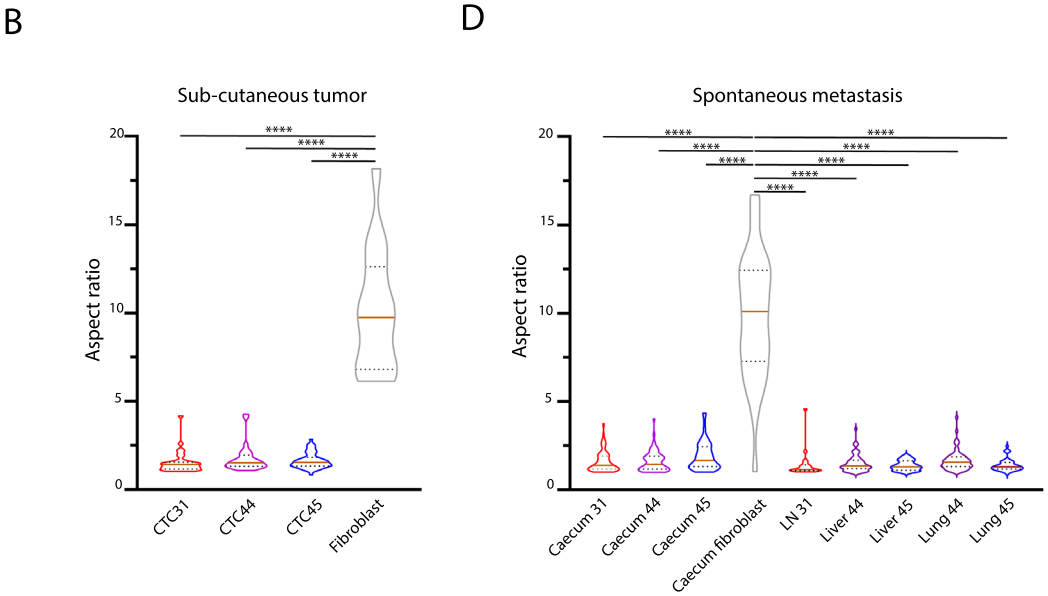

Collagen suspension for live cell imaging

CTC single cells were embedded in a low-density bovine collagen (1.7 mg/mL, 20µm^2). After collagen polymerization, (37°C, 10 – 20 min), drops were covered by cell culture M12 medium and placed in incubator with 21% normoxic oxygen levels as previously described[36]. For single cell detachment, spheres were grown on average 7 days in collagen in a well containing at least 1 ml of medium, refreshed every 24 h. CTC growth was dependent on the CTC line. Thereby, detached single cells and clusters can be observed from day 3 to day 5 post embedding. Spheres or detached single cells were imaged by an Okolab 10 × high resolution for 24 h.

◀**Fig. 3**. CTC lines keep a round epithelial morphology in in vivo models. (**A**) Representative pictures of immunohistochemistry using CK20 antibody on subcutaneous tumor sections generated by each CTC line in 3 different mice. Black arrows and gray arrows indicate a single detached cell and a cluster detached from the tumor bulk respectively. Scale bar = 50 µm. (**B**) Violin plot of the aspect ratio of a detached single cell in subcutaneous tumor generated by each CTC line. CTC31, 33 detached single cells; CTC44, 30 detached single cells; CTC45, 51 detached single cells; fibroblast, 15 from all subcutaneous tumors. Brown bar, mean; Dotted line, quartiles. ****P < 0.0001, Mann–Whitney test. Aspect ratio measured by dividing length by the width. (**C**) Representative pictures of immunohistochemistry using CK20 or P-mito antibodies on orthotopic caecum tumor sections (left column) and colonized distant organs (right column) as lymph node (top right) or liver sections generated by each CTC line. Black arrows and gray arrows indicate a single detached cell and a cluster detached from the tumor bulk respectively. Scale bar = 50 µm (n = 2 to 3 mice per CTC line). (**D**) Violin plot of the aspect ratio of a detached single cell in primary caecum tumor and in distant organs generated by each CTC line. CTC31 caecum, 117 detached single cells; CTC44 cecum, 59 detached single cells; CTC45 cecum, 61 detached single cells; caecum fibroblast, 29 from all caecum; CTC31 lymph node, 20 detached single cells; CTC44 liver, 57 detached single cells; CTC45 liver, 18 detached single cells. Brown bar, mean; Dotted line, quartiles. ****P < 0.0001, Mann–Whitney test.

Cytometry

CTC31 spheres were centrifuged at 300 g for 5 min, and the supernatant was removed. Pellets were suspended with an equal volume of Accumax (A7089-100ML Sigma-Aldrich, St Louis, MO, USA). Spheres were then gently mixed and incubated at 37 °C for 30 to 45 min according to the sphere size. For Accumax inactivation, 3 mL of blocking buffer was added and cells were incubated on ice for 10 min. This blocking buffer contains the auto MACS rinsing solution (130–091-222, Miltenyi Biotec) with 1% of BSA (130–091-376, Miltenyi Biotec). Cells were filtred through a 40 µm Falcon Cell Strainer before counting and staining. 200 000 cells per condition were collected and stained with PE-conjugated EpCAM antibody (130–111-116, Miltenyi Biotec) or with PE-conjugated isotype antibody (130–104-612, Miltenyi Biotec) and then analyzed using BD LSR Fortessa with BD FACSDiva 8.0 Software. Dead cells were excluded with SytoxBlue (S34857, ThermoFisher).

Migration assay with xCELLigence

Cell migration assays were conducted using the label-free Real-Time Cell Analyzer (RTCA) platform (xCELLigence, Agilent) using 8 µm pore migration plates containing 16 wells (CIM-plate 16). Wells are formed by a lower and an upper chamber placed at 37 °C and 5% CO2. The system assesses the impact of inhibiting actomyosin contractility, a characteristic feature of amoeboid migration, on circulating tumor cell (CTC) behavior through the use of Y27632 (StemCell #72,302), a Rho/ROCK inhibitor. For these assays, 40,000 cells were seeded per well in the upper chamber of a CIM-plate 16, either treated with Y27632 (10 µM) or left untreated. Both the upper and lower chambers contained DMEM medium (Gibco) supplemented with 10% FBS (Eurobio). The xCELLigence system automatically recorded the electrical impedance value of each well every 15 min over a 24-h period, reflecting cell-microelectrode contact, further interpreted as a Cell Index (CI) value. Biological replicates were performed three times. Despite significant variability inherent to the xCELLigence technology when applied to CTCs, a consistent trend was observed: the presence of the ROCK inhibitor constantly reduced CTC migration. The results presented are from one representative experiment, as combining the triplicate data was not technically feasible.

In vivo assay

All mice were housed in a SPF environment. All animal experiments were approved by the French Agriculture and Forestry Ministry (Authorization referral: B 34–172-41). The methods complied to the guidelines and regulations of the French Agriculture and Forestry Ministry and the ARRIVE guidelines. At the end of both in vivo experiments, The mice are euthanized by CO_2 asphyxiation or by cervical dislocation.

Subcutaneous injection

200,000 cells from CTC lines were subcutaneously injected into the right flanks of 6-week-old female nude mice (Charles River, France). The cells were suspended in a 1:1 mixture of Matrigel (Corning 356,231) and DMEM (Gibco), with a final volume of 50 µL. Tumor growth was monitored over time by caliper measurements performed twice a week for subcutaneous xenografts. Tumor is harvested once the volume reach 1000 mm^3. Mice were received at 20 g of body weight and euthanized around 30 g of body weight. Subcutaneous injection did not impact mice weight.

Intracaecal injection

First, cells were transfected with the firefly luciferase vector pGL3 (Promega Corporation). Then, 2 million CTCs resuspended in a 50% DMEM and Matrigel mixture with a final volume of 10 µL were injected into the caecal wall as described by[47]. Briefly, a subcutaneous injection (25G needle) of buprenorphine (0.05 mg/kg) 30–45 min beforehand, anaesthesia with isoflurane (1.5–3%) delivered via mask, and placement on a heating pad at 37 °C. Buprenorphine is administered twice daily to provide analgesic effects. The animal is rehydrated with 0.9% saline solution by a subcutaneous injection of 300 µL. The surgical area is first washed and disinfected (three times: soap, water, and Betadine) and then locally anesthetized with lidocaine spray. Deep anaesthesia is verified by pinching the paw. All surgical instruments are sterilized beforehand. The skin and abdominal wall are incised, and a sterile surgical drape is placed to maintain a sterile field.

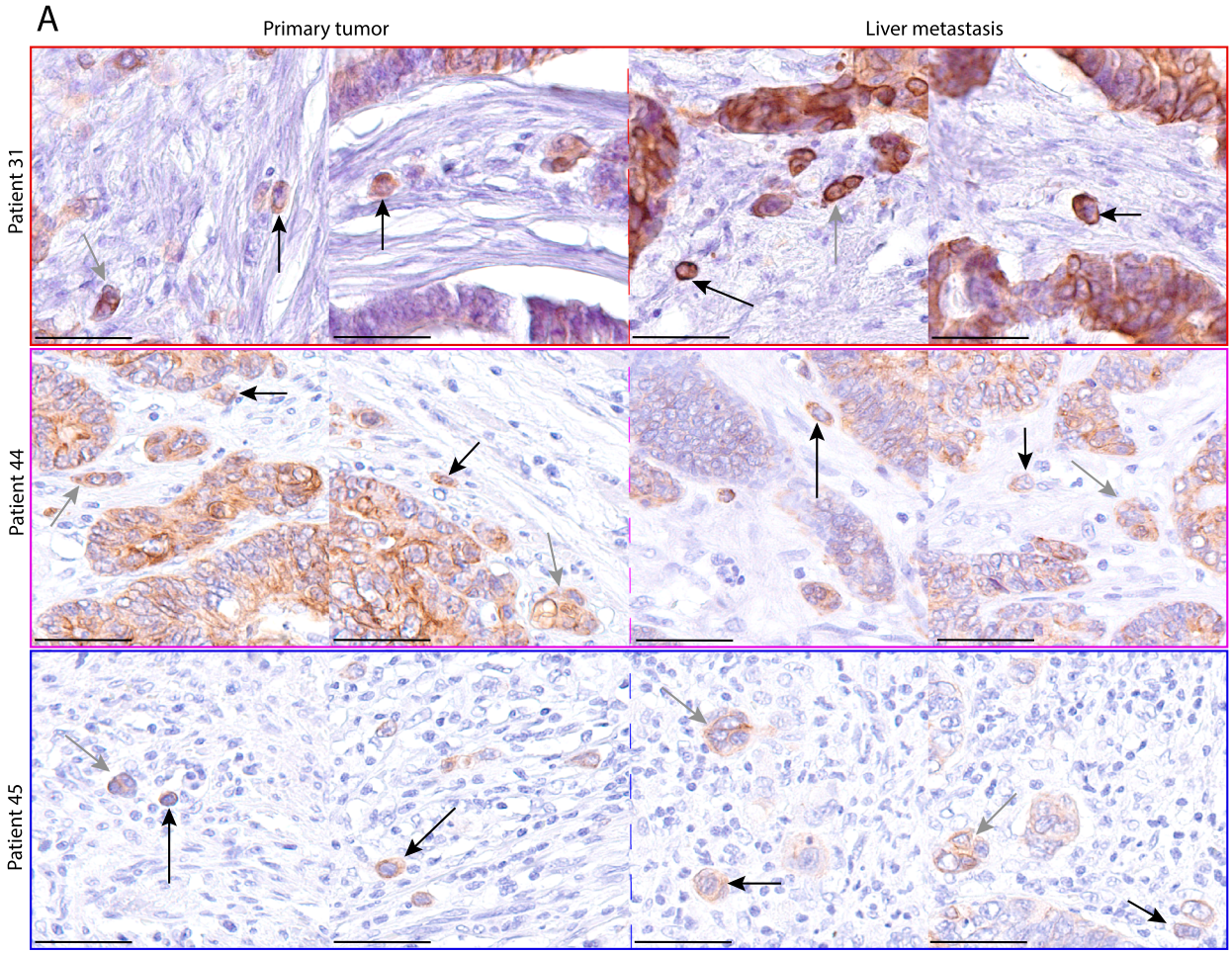

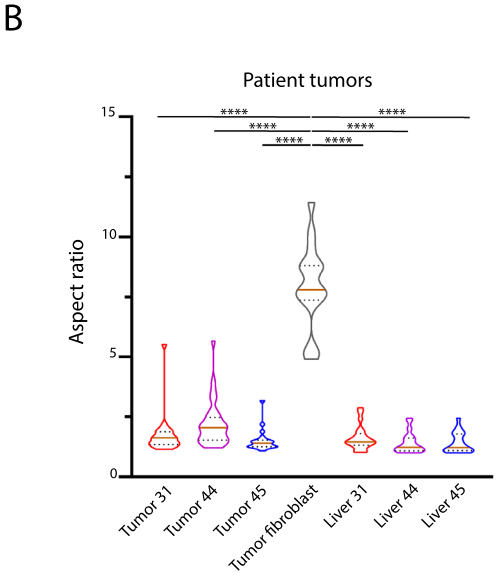

Monitoring was performed with an IVIS200 (Xenogen). Mice were intra peritoneally injected with 150 mg/Kg of luciferin (Caliper Life Sciences) mixed with PBS. After 10 min, animals were anaesthetized and imaged. Animals were sacrificed when the bioluminescence signal of the primary tumor reached 4.5×10^6 photons/s or at 12 weeks after grafting. Then, organs were collected for fixation.

Immunohistochemistry and image analysis (for aspect ratio)

Slides were processed as for immunofluorescent with an additional step requiring an incubation with 1.5% H2O2 in methanol for 20 min to quench endogenous peroxydase activity. CK20 antibody was purchased from Abcam

◀**Fig. 4**. Invading cells in patients also show a round and epithelial morphology. (**A**) Representative pictures of immunohistochemistry using CK20 antibody on colorectal primary tumor sections (left columns) and liver metastasis (right columns) from patients from whose CPP and CTC lines have been generated. Black arrows and gray arrows indicate a single detached cell and a cluster detached from the tumor bulk respectively. Scale bar = 50 µm. (**B**) Violin plot of the aspect ratio of detached single cells in colorectal primary tumors and in corresponding liver metastasis. Primary tumor **#31**, 21 detached single cells; primary tumor **#44**, 33 detached single cells; primary tumor **#45**, 20 detached single cells; primary tumor fibroblast, 16 from all colorectal primary tumors; liver metastasis **#31**, 21 detached single cells; liver metastasis **#44**, 33 detached single cells; liver metastasis **#45**, 20 detached single cells. Brown bar, mean; Dotted line, quartiles. **** $P < 0.0001$, Mann–Whitney test.

(ab76126) and P-Mito from Sigma (MAB1273). ImmPRESS® HRP Goat Anti-Rabbit IgG Polymer Detection Kit, Peroxidase (MP-7451) was used as a secondary reagent. The signal was developed with DAB (Sigma-Aldrich). Slides were then counterstained with hematoxylin (DiaPath), dehydrated, and mounted in Pertex (Histolab). Hamamatsu nanozoomer was used for scanning.

Data availability

The datasets used and/or analyzed in the current study are available from the corresponding author upon reasonable request. However, all the RNA seq data, package and signatures used are publically accessible as describe in the Methods section.

Received: 27 October 2025; Accepted: 27 March 2026
Published online: 29 April 2026

References

1. Mehlen, P. & Puisieux, A. Metastasis: A question of life or death. *Nat. Rev. Cancer* **6**(6), 449–458 (2006).
2. Xi, Y. & Xu, P. Global colorectal cancer burden in 2020 and projections to 2040. *Transl. Oncol.* **14**(10), 101174 (2021).
3. ASCO. *Colorectal Cancer: Statistics*. Cancer. Net 2023; Available from: https://www.cancer.net/cancer-types/colorectal-cancer/statistics (2023).
4. Cohen, S. J. et al. Relationship of circulating tumor cells to tumor response, progression-free survival, and overall survival in patients with metastatic colorectal cancer. *J. Clin. Oncol.* **26**(19), 3213–3221 (2008).
5. Yu, M. et al. Circulating breast tumor cells exhibit dynamic changes in epithelial and mesenchymal composition. *Science* **339**(6119), 580–584 (2013).
6. Gkountela, S. et al. Circulating tumor cell clustering shapes DNA methylation to enable metastasis seeding. *Cell* **176**(1–2), 98-112. e14 (2019).
7. Grillet, F. et al. Circulating tumour cells from patients with colorectal cancer have cancer stem cell hallmarks in ex vivo culture. *Gut* **66**(10), 1802–1810 (2017).
8. Chaffer, C. L. et al. EMT, cell plasticity and metastasis. *Cancer Metastasis Rev.* **35**(4), 645–654 (2016).
9. Fischer, K. R. et al. Epithelial-to-mesenchymal transition is not required for lung metastasis but contributes to chemoresistance. *Nature* **527**(7579), 472–476 (2015).
10. Chen, Y. et al. Circulating tumor cells undergoing EMT are poorly correlated with clinical stages or predictive of recurrence in hepatocellular carcinoma. *Sci. Rep.* **9**(1), 7084 (2019).
11. Papadaki, M. A. et al. Circulating tumor cells with stemness and epithelial-to-mesenchymal transition features are chemoresistant and predictive of poor outcome in metastatic breast cancer. *Mol. Cancer Ther.* **18**(2), 437–447 (2019).
12. Brooks, P. C. et al. Localization of matrix metalloproteinase MMP-2 to the surface of invasive cells by interaction with integrin αvβ3. *Cell* **85**(5), 683–693 (1996).
13. Friedl, P. & Wolf, K. Tumour-cell invasion and migration: Diversity and escape mechanisms. *Nat. Rev. Cancer* **3**(5), 362–374 (2003).
14. Wolf, K. et al. Compensation mechanism in tumor cell migration. *J. Cell Biol.* **160**(2), 267–277 (2003).
15. Sahai, E. & Marshall, C. J. Differing modes of tumour cell invasion have distinct requirements for Rho/ROCK signalling and extracellular proteolysis. *Nat. Cell Biol.* **5**(8), 711–719 (2003).
16. Wyckoff, J. B. et al. ROCK- and myosin-dependent matrix deformation enables protease-independent tumor-cell invasion in vivo. *Curr. Biol.* **16**(15), 1515–1523 (2006).
17. Friedl, P. & Bröcker, E. B. The biology of cell locomotion within three-dimensional extracellular matrix. *Cell. Mol. Life Sci. (CMLS)* **57**(1), 41–64 (2000).
18. Friedl, P. et al. Classifying collective cancer cell invasion. *Nat. Cell Biol.* **14**(8), 777–783 (2012).
19. Pandya, P., Orgaz, J. L. & Sanz-Moreno, V. Modes of invasion during tumour dissemination. *Mol. Oncol.* **11**(1), 5–27 (2017).
20. Tognoli, M. L. et al. RASSF1C oncogene elicits amoeboid invasion, cancer stemness, and extracellular vesicle release via a SRC/Rho axis. *EMBO J.* **40**(20), EMBJ2021107680 (2021).
21. Laser-Azogui, A. et al. Met-induced membrane blebbing leads to amoeboid cell motility and invasion. *Oncogene* **33**(14), 1788–1798 (2014).
22. Di Raimo, T. et al. Circulating tumor cells and the metastatic process: The complexity of malignancy. *J. Cancer Metastasis Treat.* **4**(10), 54 (2018).
23. Pagès, D.-L. et al. Cell clusters adopt a collective amoeboid mode of migration in confined nonadhesive environments. *Sci. Adv.* **8**(39), eabp841 (2022).
24. Tan, T. Z. et al. Epithelial-mesenchymal transition spectrum quantification and its efficacy in deciphering survival and drug responses of cancer patients. *EMBO Mol. Med.* **6**(10), 1279–1293 (2014).
25. Foroutan, M. et al. A transcriptional program for detecting TGFβ-induced EMT in cancer. *Mol. Cancer Res.* **15**(5), 619–631 (2017).
26. Čermák, V. et al. RNA-seq of macrophages of amoeboid or mesenchymal migratory phenotype due to specific structure of environment. *Sci. Data.* **5**(1), 180198 (2018).
27. Foroutan, M. et al. Single sample scoring of molecular phenotypes. *BMC Bioinformatics* **19**(1), 404 (2018).
28. Samain, R. et al. CD73 controls Myosin II–driven invasion, metastasis, and immunosuppression in amoeboid pancreatic cancer cells. *Sci. Adv.* **9**(42), eadi0244 (2023).
29. Belthier, G. et al. CD44v6 defines a new population of circulating tumor cells not expressing EpCAM. *Cancers* **13**(19), 4966 (2021).

30. Weigelin, B., Bakker, G.-J. & Friedl, P. Intravital third harmonic generation microscopy of collective melanoma cell invasion. *IntraVital* **1**(1), 32–43 (2012).
31. Lehmann, S. et al. Hypoxia induces a HIF-1-dependent transition from collective-to-amoeboid dissemination in epithelial cancer cells. *Curr. Biol.* **27**(3), 392–400 (2017).
32. Wolf, K. et al. Amoeboid shape change and contact guidance: T-lymphocyte crawling through fibrillar collagen is independent of matrix remodeling by MMPs and other proteases. *Blood* **102**(9), 3262–3269 (2003).
33. Shiozawa, Y. et al. Cancer stem cells and their role in metastasis. *Pharmacol. Ther.* **138**(2), 285–293 (2013).
34. Shibue, T. & Weinberg, R. A. EMT, CSCs, and drug resistance: The mechanistic link and clinical implications. *Nat. Rev. Clin. Oncol.* **14**(10), 611–629 (2017).
35. Sanz-Moreno, V. et al. Rac activation and inactivation control plasticity of tumor cell movement. *Cell* **135**(3), 510–523 (2008).
36. te Boekhorst, V. et al. Calpain-2 regulates hypoxia/HIF-induced plasticity toward amoeboid cancer cell migration and metastasis. *Curr. Biol.* **32**(2), 412–427 (2022).
37. Sahai, E. et al. Smurf1 regulates tumor cell plasticity and motility through degradation of RhoA leading to localized inhibition of contractility. *J. Cell Biol.* **176**(1), 35–42 (2007).
38. Huang, Y. et al. Evaluation of cancer stem cell migration using compartmentalizing microfluidic devices and live cell imaging. *J. Vis. Exp.* **2011**(58), 3297 (2011).
39. Taddei, M. L. et al. Mesenchymal to amoeboid transition is associated with stem-like features of melanoma cells. *Cell Commun. Signal.* **12**(1), 24 (2014).
40. Chikina, A. S. et al. Transition from mesenchymal to bleb-based motility is predominantly exhibited by CD133-positive subpopulation of fibrosarcoma cells. *Biol. Cell* **111**(10), 245–261 (2019).
41. Emad, A. et al. Superior breast cancer metastasis risk stratification using an epithelial-mesenchymal-amoeboid transition gene signature. *Breast Cancer Res.* **22**(1), 74 (2020).
42. Graziani, V. et al. The amoeboid state as part of the epithelial-to-mesenchymal transition programme. *Trends Cell Biol.* **32**(3), 228–242 (2022).
43. Wu, J.-S. et al. Plasticity of cancer cell invasion: Patterns and mechanisms. *Transl. Oncol.* **14**(1), 100899 (2021).
44. Crosas-Molist, E. et al. The NADPH oxidase NOX4 represses epithelial to amoeboid transition and efficient tumour dissemination. *Oncogene* **36**(21), 3002–3014 (2017).
45. López-Luque, J. et al. Downregulation of epidermal growth factor receptor in hepatocellular carcinoma facilitates transforming growth factor-β-induced epithelial to amoeboid transition. *Cancer Lett.* **464**, 15–24 (2019).
46. Robinson, M. D., Mccarthy, D. J. & Smyth, G. K. *edgeR*: A Bioconductor package for differential expression analysis of digital gene expression data. *Bioinformatics* **26**(1), 139–140 (2010).
47. Hackl, C. et al. Metronomic oral topotecan prolongs survival and reduces liver metastasis in improved preclinical orthotopic and adjuvant therapy colon cancer models. *Gut* **62**, 259–271 (2013).

Acknowledgements

Authors would like to acknowledge iexplore facilities (RAM) and the imaging facility MRI.

Author contributions

Conceptualization, G.B, F.G, V.t.B, P.F, and J.P. Methodology, G.B, F.G., V.t.B, H.M, M.A.A, F.H, P.F and J.P; Investigation, F.G, V.t.B, G.B, M.A.A. M.F. Z.H, J.V.B, G.D.S, L.CT. Formal Analysis; V.t.B, G.B, M.A.A, M.F, H.M, P.F and J.P Writing – Original Draft & Editing, G.B, Z.H, V.t.B, J.V.B, M.A.A, H.M, P.F and J.P; Funding Acquisition, Z.H., GB., and J.P; Resources, JF.B, M.P, E.S, T.M, G.L, L.K, F.H ; Supervision, P.F and J.P.

Fundings

This research was publicly funded through the I-SITE Excellence Program of the University of Montpellier, part of the Investments France 2030; Institut national du cancer (INCA, PLBIO22-084), SIRIC: Grant "INCa-DGOS-Inserm 6045" and ITMO Cancer (MCMP 2024, C24015FS). ZH has been funded by "fondation pour la recherche médicale" and ZH, FG and GB have been funded by "la ligue contre le cancer".V.t.B. was supported by the Rosalie B. Hite Fellowship for Cancer Research.

Declaration

Competing interests

The authors declare no competing interests.

Ethics approval

Patient CTC and tumor-derived cell lines (CTC 44, 45 and CPP 44 and 45) were obtained from CRC patient blood and biopsies provided by CHU-Carémeau (Nîmes, France, ClinicalTrial.gov Identifier#NCT01577511). Patient CTC 31 cell line was obtained from a CRC patient blood sample provided by Montpellier Cancer Institute (Institut du Cancer de Montpellier; ICM) under the ethics agreement number 2016-A00080-51. Established cell lines were used in accordance to the clinical trial guidelines.

Patient consent

Obtained for both clinical trials listed below at the time of sample collections.

Additional information

Supplementary Information The online version contains supplementary material available at https://doi.org/10.1038/s41598-026-46858-3.

Correspondence and requests for materials should be addressed to J.P.